Atmosphere-Ocean

ISSN: 0705-5900 (Print) 1480-9214 (Online) Journal homepage: http://www.tandfonline.com/loi/tato20

Interdecadal Variability of the ENSO–North Pacific Atmospheric Circulation in Winter

Peng Zhang, Zhiwei Wu & Hua Chen

To cite this article: Peng Zhang, Zhiwei Wu & Hua Chen (2017) Interdecadal Variability of the ENSO–North Pacific Atmospheric Circulation in Winter, Atmosphere-Ocean, 55:2, 110-120, DOI: 10.1080/07055900.2017.1291411

To link to this article: https://doi.org/10.1080/07055900.2017.1291411

Published online: 07 Mar 2017.

Interdecadal Variability of the ENSO–North Pacific Atmospheric Circulation in Winter

Peng Zhang[1], Zhiwei Wu[2,*], and Hua Chen[1]

[1]*College of Atmospheric Science and Key Laboratory of Meteorological Disaster of Ministry of Education, Nanjing University of Information Science & Technology, Nanjing, Jiangsu 210044, China*

[2]*Institute of Atmospheric Sciences, Fudan University, Shanghai 200433, China*

[Original manuscript received 21 June 2016; accepted 3 January 2017]

ABSTRACT *The interdecadal change in the relationship between the El Niño–Southern Oscillation (ENSO) and atmospheric circulation over the North Pacific is investigated using both observational data and an atmospheric general circulation model. There are two prominent modes of winter mid-latitude atmospheric variability in the North Pacific: the West Pacific (WP) teleconnection and the Aleutian Low (AL). The relationship between ENSO and the WP-AL patterns changed notably around the late 1970s. From 1957 to 1975, during the mature phase of ENSO, significant sea surface temperature anomalies (SSTAs) occurred, mainly in the equatorial eastern Pacific Ocean; the associated atmospheric circulation anomaly pattern resembles the negative phase of a WP teleconnection pattern. In contrast, for the 1978–2011 period, significant negative SSTAs were observed in the western and extratropical Pacific in both hemispheres, with some significant positive SSTAs appearing over the eastern Pacific. This is in agreement with the defined regions of a mega-ENSO, the associated atmospheric circulation anomaly pattern resembles the AL mode. Further analysis suggests that a negative–positive anomaly pattern in the 500 hPa geopotential height throughout the entire North Pacific, possibly enhanced by the SSTAs in the extratropical North Pacific associated with the mature phase of ENSO, is responsible for modulating the relationship between ENSO and the North Pacific atmospheric circulation.*

RÉSUMÉ *[Traduit par la rédaction] Nous étudions la modification interdécennale de la relation entre le phénomène El Niño-oscillation australe (ENSO) et la circulation atmosphérique sur le Pacifique Nord, et ce, à l'aide d'observations et de données issues d'un modèle de circulation générale de l'atmosphère. Il existe deux modes dominants de variabilité dans le nord du Pacifique : la téléconnexion du Pacifique Ouest et la dépression des Aléoutiennes. La relation entre l'ENSO et les configurations liées au phénomène du Pacifique Ouest et à la dépression des Aléoutiennes a considérablement changé vers la fin des années 1970. De 1957 à 1975, durant la phase de maturité de l'ENSO, des anomalies notables de températures de surface de la mer (SST) sont survenues principalement dans l'est équatorial de l'océan Pacifique. La circulation atmosphérique anomale associée ressemble à la phase négative de la téléconnexion du Pacifique Ouest. En revanche, de 1978 à 2011, des anomalies négatives notables de SST ont été observées dans le Pacifique Ouest et extratropical, dans les deux hémisphères. Des anomalies positives notables de SST sont aussi survenues dans l'est du Pacifique. Ces emplacements correspondent aux régions propices à un important ENSO. La circulation atmosphérique anomale associée ressemble au mode de la dépression des Aléoutiennes. Des analyses subséquentes laissent penser qu'une configuration d'anomalies négatives et positives des hauteurs géopotentielles à 500 hPa sur le nord du Pacifique, possiblement renforcée par des anomalies de SST associées à la phase de maturité de l'ENSO, dans la région nord extratropicale du Pacifique, module la relation entre l'ENSO et la circulation atmosphérique du Pacifique Nord.*

KEYWORDS ENSO; North Pacific; interdecadal variability; Aleutian Low; West Pacific teleconnection

1 Introduction

Climate variability in the North Pacific has drawn considerable attention in recent years because of its impact on tropical and extratropical regions (Barlow, Nigam, & Berbery, 2001; Ceballos et al., 2009; Deser, Alexander, & Timlin, 1999; Graham, 1994; He, Wang, & Liu, 2013; Hsu & Wallace, 1985; Latif & Barnett, 1994, 1996; Oshika, Tachibana, & Nakamura, 2014). There are two dominant modes of atmospheric variability over the North Pacific. One is linked to changes in the Aleutian Low (AL; Trenberth & Hurrell, 1994), the other to the North Pacific Oscillation (NPO; Rogers, 1981; Walker & Bliss, 1932), with the upper-tropospheric

*Corresponding author's Email: zhiweiwu@fudan.edu.cn

geopotential height displaying the West Pacific (WP) teleconnection pattern (Linkin & Nigam, 2008; Wallace & Gutzler, 1981). The winter variability of the AL is associated with the Pacific–North American (PNA) teleconnection and the variability of the circulation around the Arctic as the Arctic Oscillation (Overland, Adams, & Bond, 1999). Its influence in the northern hemisphere is evident from the surface (Maslanik, Serreze, & Barry, 1996) to the stratosphere (Kodera, Chiba, Koide, Kitoh, & Nikaidou, 1996). Compared with the PNA pattern, the WP pattern has received little research attention, despite its significant influence on winter continental precipitation (Linkin & Nigam, 2008; Nigam, 2003). The negative phase of the WP pattern affects the East Asian monsoon and leads to abnormally cool temperatures over eastern Eurasia in the winter (Gong, Wang, & Zhu, 2001; Zhang et al., 2009).

The El Niño–Southern Oscillation (ENSO) is one of the most important factors influencing the world climate. There are many studies on ENSO and its impacts on climate (Charney & Shukla, 1981; Chang, Zhang, & Li, 2000; Jin, Neelin, & Ghil, 1994; Neelin et al., 1998; Ropelewski & Halpert, 1986; Wang, Wu, & Fu, 2000, 2008; Wu & Li, 2008, 2009; Wu & Lin, 2012; Wu, Wang, Li, & Jin, 2009; Zhang et al., 1996 and many others). The association of ENSO with atmospheric circulation over the North Pacific has also been widely examined. Previous studies have shown that the boreal winter near-surface atmospheric circulation over the North and central Pacific influences the state of the tropical Pacific and initiates the development of ENSO events (Anderson et al., 2013; Anderson & Renellys, 2015). Conversely, the circulation over the North Pacific is also affected by tropical sea surface temperature anomalies (SSTAs). Bjerknes (1966, 1969) first noted that the AL tended to strengthen and shift southeastward during El Niño events. Trenberth and Hurrell (1994) found that the deepened AL during ENSO events resulted in a characteristic SSTA pattern that, on average, was enhanced through the effects of extratropical SSTAs themselves. Meanwhile, ENSO is also a well-known key factor in the long-term prediction of the WP pattern (Horel & Wallace, 1981; Kodera, 1998; Mo & Livezey, 1986; Oshika et al., 2014). Horel and Wallace (1981) showed that winter El Niño events are associated with the positive phase of the winter WP pattern.

There is evidence of a decade-long change in the North Pacific atmosphere and ocean beginning in the mid-1970s (Hanawa, Ishizaki, & Tanimoto, 1996; Overland et al., 1999; Trenberth, 1990; Trenberth & Hurrell, 1994). The oceanic change is characterized by cooling SSTAs in the central and western North Pacific and warming SSTAs in the eastern tropical Pacific (Deser, Alexander, & Timlin, 1996; Guilderson & Schrag, 1998; Trenberth, 1990). The atmospheric change includes an intensification and eastward shift of the AL (Graham, 1994; Trenberth, 1990; Trenberth & Hurrell, 1994). Such interdecadal changes of the ocean–atmosphere system could strongly affect the interannual relationship between tropical SSTAs and atmospheric circulation and further impact regional climate, such as the East Asian winter monsoon (Ding, Ha, & Li, 2010; He & Wang, 2013). Thus, understanding interdecadal changes in the relationship between ENSO and the WP pattern and the AL is of great importance for seasonal climate prediction. In addition, the possible physical mechanisms responsible for the interdecadal variability of the ENSO–North Pacific atmospheric circulation are unclear. We try to provide some explanation in this study. Our paper is structured as follows. Section 2 describes the data, model, and experimental design. The distinctive ENSO-related atmospheric circulation anomalies between 1957–1975 and 1978–2011 are examined in Section 3. Section 4 compares the differences between the three-dimensional circulation structures associated with ENSO during these two epochs. In Section 5, the modulating effect of the extratropical North Pacific (XNP) SSTAs is discussed, and an atmospheric general circulation model (AGCM) is utilized to assess the mechanisms. The last section summarizes the paper.

2 Data, model, and experiments

The data used in this study include (i) monthly mean atmospheric fields from the National Oceanic and Atmospheric Administration–Cooperative Institute for Research in Environmental Sciences (NOAA–CIRES) twentieth century reanalysis project for the period 1871–2012 (20th-RC; Compo, Whitaker, & Sardeshmukh, 2006, 2011; Whitaker, Compo, Wei, & Hamill, 2004). The 1871–2012 period is used to calculate the Aleutian Low index (ALI) and the West Pacific teleconnection index (WPI). The lack of sea surface temperature (SST) and sea level pressure (SLP) observations over East Asia in the late nineteenth and early twentieth centuries (King, Alexander, & Donat, 2013; Wang et al., 2013) may affect our results (our study focuses on the 1957–2011 period); and (ii) monthly mean SST data from the Extended Reconstructed Sea Surface Temperature, version 3b (ERSST v3b; Smith, Reynolds, Peterson, & Lawrimore, 2008) dataset.

The definition of the WPI follows the description in Oshika et al. (2014). The time series of the first leading mode of the December, January, February (DJF) geopotential height at 500 hPa (Z500) in the western Pacific region (20°N–80°N, 120°E–180°) is used as the WPI. The ALI is defined as the area-weighted SLP over the region 30°N–70°N, 155°E–130°W (He et al., 2013). The spatial patterns of the AL and WP modes at 500 hPa are shown in Fig. 1. The Pacific Decadal Oscillation (PDO) index used in this study is constructed according to the definition given by Mantua, Hare, Zhang, Wallace, and Francis (1997), which is defined as the first leading empirical orthogonal function (EOF) mode of the detrended monthly SSTAs over 20°–60°N, 120°E–120°W. Finally, the Interdecadal Pacific Oscillation (IPO) index is consistent with the definition given by Dai (2013), which is the second leading EOF of the three-year moving-average global SSTs. To emphasize the interannual variability, we

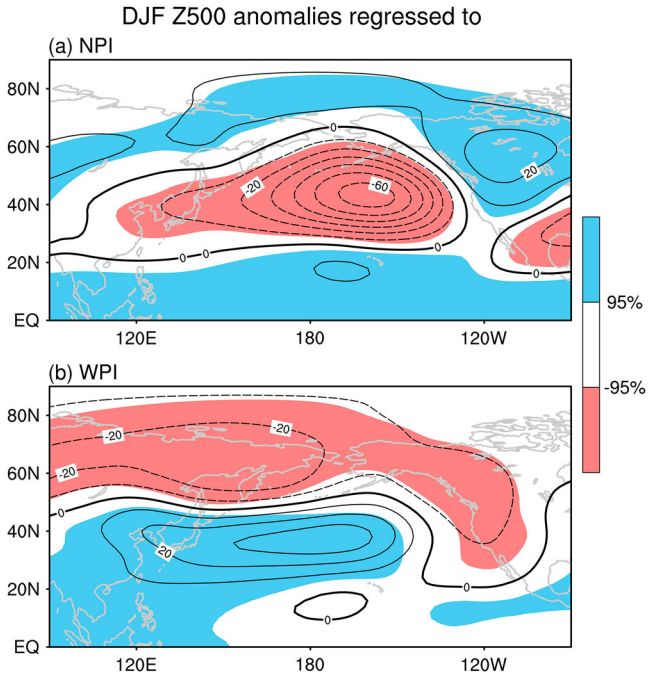

Fig. 1 December, January, and February (DJF) 500 hPa geopotential height (Z500) anomalies regressed against (a) the ALI (contour intervals are 10 gpm); (b) the WPI from 1957 to 2011. Values in the shaded areas exceed the 95% confidence level based on a Student's *t*-test.

removed the linear trends from the aforementioned datasets. The effective degree of freedom (DOF) is determined using the method outlined in Bretherton, Widmann, Dymnikov, Wallace, and Blade (1999).

$$N^* = N[(1 - R_1R_2)/(1 + R_1R_2)],$$

where N^* is the effective sample size, N is the original sample size, R_1 and R_2 are the lag-1 autocorrelation coefficients of the two time series involved. Because the tropical Pacific SSTAs have experienced a notable interdecadal change in their connection with the winter WP pattern or AL during the past 55 years. The effective DOF of the WPI and ALI in the two subperiods as well as for the entire period are calculated separately (Table 1). In the following, $N^* = 0.78N$ is used for all indices such that the significance test is more strict for each variable.

The numerical experiments were performed with an AGCM, the 5th generation European Centre–Max Plank Institute model (ECHAM), v5.4 (Roeckner et al., 2003). We used T63L19; this version features a horizontal resolution of 1.875° and 19 vertical levels. The SST forcing fields were derived from the Atmospheric Model Intercomparison Project (AMIP) II SST and sea-ice concentration boundary conditions. Four experiments were designed. First, a control experiment was run in which AMIP II time-varying historical SSTs were used; the simulation was continually integrated for 10 years from 1966 to 1975, and the results from the last 8 years (31 December 1967 to 28 February 1975) were used as the samples. Then, the SSTA sensitivity experiments were run, for which observational SSTAs were added to the DJF historical SSTs, and the simulations were integrated from 31 October to 28 February of the following year with the initial conditions taken from the control experiment. The first sensitivity experiment was forced by the DJF historical SSTs plus the DJF SST differences between the warm (normalized Niño 3.4 index greater than 0.5) and cold (normalized Niño 3.4 index less than 0.5) ENSOs for the 1978–2011 period. We imposed such mega-ENSO type SSTAs over the region 0°–360°E, 40°S–60°N to mimic the coupled effect of XNP and eastern equatorial Pacific SSTAs. The second sensitivity experiment was similar to the first one, but we removed the SSTAs in the extratropical Pacific against the background of a mega-ENSO (0°–360°E, 15°S–15°N), which could eliminate the diabatic heating effect of the XNP forcing. In the third sensitivity experiment, we restricted the SSTA forcing in the XNP (120°–210°E, 15°–40°N) to mimic the effect of the local negative SSTAs. Last, an eight-member ensemble (arithmetic) mean was constructed to reduce the uncertainties arising from differing initial conditions and the effect of the ENSO years. Here, the control run can be regarded as an ENSO-neutral condition and the sensitivity run as the influence of a mega-ENSO, conventional ENSO, or XNP SSTAs.

TABLE 1. The lag-1 autocorrelation coefficients for the corresponding WPI and ALI and the ratio of N^* to N (in brackets).

	1957–1975	1978–2011	1957–2011
ALI	–0.35 (0.78)	–0.11 (0.97)	0.03 (0.99)
WPI	–0.21 (0.91)	0.23 (0.9)	–0.05 (0.99)

3 Interdecadal changes in the relationship between ENSO and the WP-AL patterns

In Fig. 2a, the 21-year sliding correlations of the Niño 3.4 index with the ALI and WPI show that the ENSO–WP and ENSO–AL are out of phase during the 1930–2011 period. There is a pronounced change in the correlations during the mid-1950s and mid-1970s. This is in agreement with He et al. (2013) and Wang and Kumar (2015), who found a change in the relationship between ENSO and the Asia/North America–Pacific mid-latitude winter atmospheric circulation during the mid-1970s. The temporal correlation coefficients among each index for the different periods are listed in Table 2. The ALI and the WPI are weakly correlated during each epoch, indicating that they are probably independent atmospheric systems. It should be noted that King et al. (2013) and Wang et al. (2013) mentioned that in the late nineteenth and early twentieth centuries, the lack of SST and SLP observations over East Asia may affect the results, so we contrasted the DJF Z500 anomaly responses with ENSO for the 1930–1950 and 1957–2009 periods by using the NOAA–CIRES long-term dataset (20th-CR, 1871–2012, 2° × 2°) and the European Centre for Medium-range Weather Forecasts (ECMWF) 20-year reanalysis dataset (ERA-20C, 1900–2010, 2° × 2°) (figure not shown). It shows that there is a

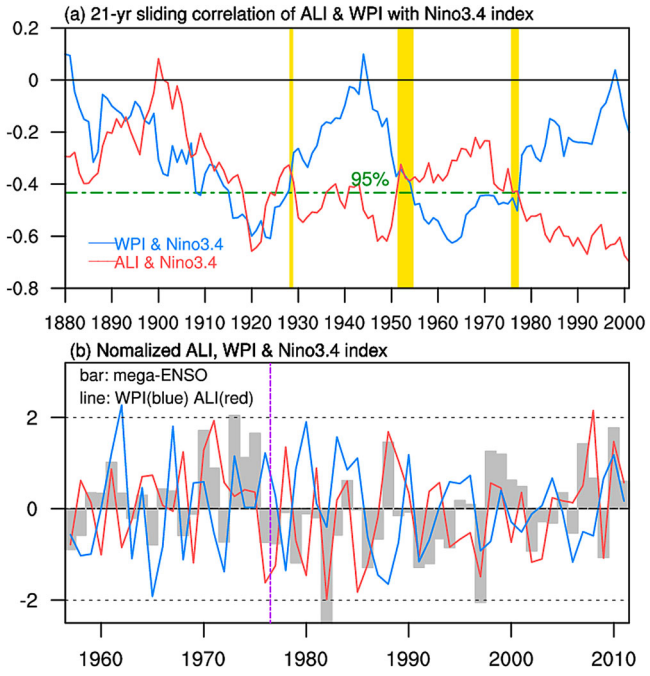

Fig. 2 (a) The 21-year sliding correlation of the Niño 3.4 index with the WP index (blue curve) and the ALI (red curve) during DJF from 1880 to 2001. The horizontal dashed line indicates values exceeding the 95% confidence level based on a Student's *t*-test. (b) Time series of the normalized ALI (black curve), WPI (red curve), and Niño 3.4 index (grey bar) in DJF for the 1957–2011 period. The yellow bars in (a) and purple line in (b) denote the transition periods when the correlations of Niño 3.4 and WPI (ALI) change.

high structural comparability between the two datasets from 1957 to 2011. But for the 1930–1950 period, substantial differences exist in eastern Russia and northeastern China (40°–70°N, 90°–140°E). Because of existing uncertainties in the datasets from the 1930s to the 1940s, we focus on the interdecadal variability of the ENSO–North Pacific atmospheric circulation for the 1957–2011 period (Fig. 2b). In the following section, two subperiods are discussed separately. One subperiod is defined from 1957 to 1975 (P1) and the other from 1978 to 2011 (P2). The first is regarded as the ENSO–WP coupling epoch and the latter as the ENSO–AL coupling epoch.

TABLE 2. Correlation coefficients among the Niño 3.4 index, WPI, and ALI.

		Niño 3.4	WPI	ALI
1930–1950	Niño 3.4	1	–0.14	–0.46*
	WPI	–0.14	1	0.37
	ALI	–0.46*	0.37	1
1957–1975	Niño 3.4	1	–0.62*	–0.05
	WPI	–0.62*	1	–0.28
	ALI	–0.05	–0.28	1
1978–2011	Niño 3.4	1	–0.18	–0.61*
	WPI	–0.18	1	–0.22
	ALI	–0.61*	–0.22	1
1957–2011	Niño 3.4	1	0.32*	0.51*
	WPI	0.32*	1	0.23
	ALI	0.51*	0.23	1

*Indicates that the correlation coefficients exceed the 95% confidence level based on a Student's *t*-test.

If the 1957–2011 period is divided into two epochs around 1976/1977, the simultaneous SSTAs related to the WPI (ALI) clearly exhibit an ENSO-like pattern during P1 (P2) (Fig. 3a and 3d). The spatial pattern in Fig. 3d displays an anomalous eastern tropical Pacific warm and western-extratropical Pacific cold structure, which resembles the spatial pattern of a mega-ENSO. A mega-ENSO is defined as the difference between the averaged SST in the WP K-shaped area and the eastern Pacific triangle area (using averaged K-shaped SST minus averaged triangle SST; the regions are outlined by the red lines in Fig. 4; Wang et al., 2013). The magnitude and patterns of ENSO-related tropical SSTAs vary between individual El Niño and La Niña episodes (Trenberth & Smith, 2009), and all ENSO episodes are accompanied by an anomalous zonal SST gradient over the west and the residual tropical Pacific Ocean (Hoell & Funk, 2013). A mega-ENSO, as a newly defined ENSO-related pattern, reflects not only the zonal SST gradient over the west–east tropical Pacific Ocean but also the meridional SST gradient over the tropical and extratropical Pacific Ocean. This has garnered attention from the scientific community (Kim & Ha, 2015; Wu & Yu, 2015; Wu & Zhang, 2014). The spatiotemporal patterns of a mega-ENSO are shown in Fig. 4. The pattern correlation coefficient (PCC) between Fig. 3d and Fig. 4 reaches –0.94 (–0.91 for Fig. 3d and the ENSO SSTA pattern) in the oceanic region, indicating that the SSTA pattern in Fig. 3d can explain around 89% (83%) of a mega-ENSO (conventional ENSO) signal. The PCC between Fig. 3a and Fig. 4 is –0.82 (–0.91 for Fig. 3a and the ENSO SSTA pattern), indicating that the SSTA pattern in Fig. 3a can only explain around 67% (83%) of the mega-ENSO (conventional ENSO) signal. However, the PCC is greatly reduced between ENSO and the WP-related SSTA pattern in P2 (Fig. 3b, PCC = –0.47). This is also the case for the correlation between ENSO and the ALI in P1 (Fig. 3c, PCC = –0.4), suggesting that the SSTA pattern in Fig. 3b and Fig. 3c can only explain approximately 22% and 16% of the ENSO signal.

The above analysis and evidence suggest that there has been a noticeable change in the linkage between the North Pacific atmospheric circulation and ENSO during the past 55 winters. To understand the origin of such interdecadal change, the spatial structure related to Niño 3.4 during the two epochs will be examined in the following sections.

4 Contrasting spatial structures of ENSO in two epochs

Figure 5 compares the large-scale Z500 anomalies associated with ENSO during the two epochs. In general, the Z500 anomalies are symmetric about the equator in the tropical zone during the two epochs. The major difference occurs in the mid-latitude North Pacific. In P1 (Fig. 5a), there is a pattern similar to the negative phase of the WP pattern over the North Pacific, with significant positive height anomalies over Kyushu and negative height anomalies over the Kamchatka Peninsula and the western coast of North America. In P2 (Fig. 5b), the positive height anomalies over Kyushu

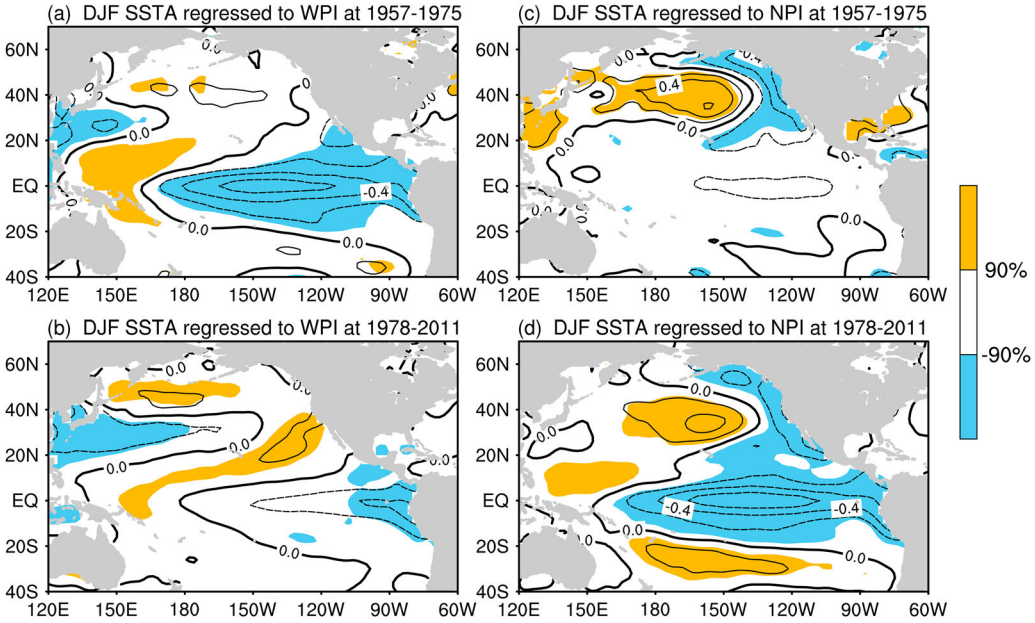

Fig. 3 1957–1975 and 1978–2011 DJF SSTA (contour intervals are 0.2 K) pattern regressed against (a) and (b) the WPI and (c) and (d) the ALI. Values in the shaded areas exceed the 90% confidence level.

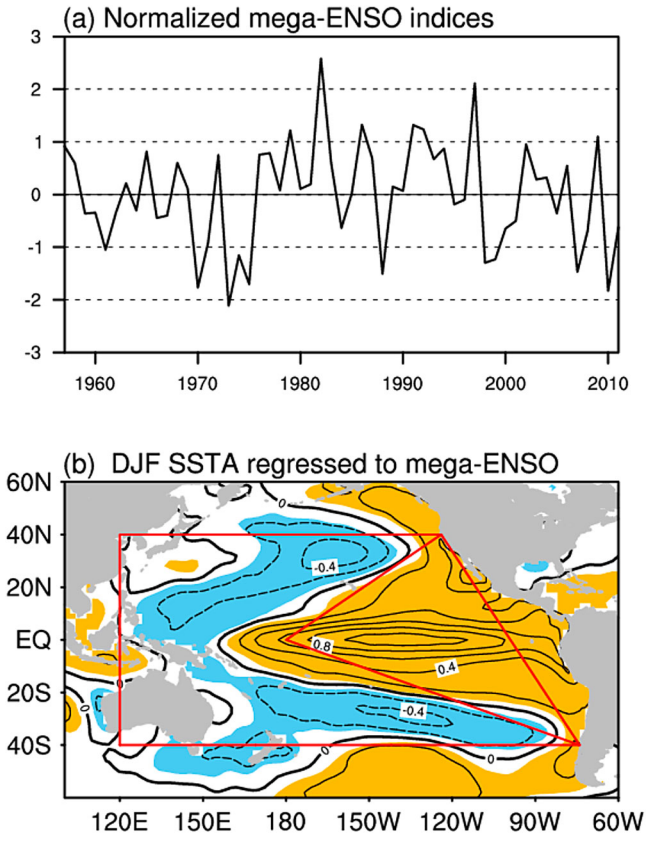

Fig. 4 (a) Time series of the normalized mega-ENSO index in DJF for the 1957–2011 period. (b) DJF SSTA regressed against the mega-ENSO index (contour intervals are 0.2 K). The shaded areas exceed the 95% confidence level based on a Student's *t*-test. The red lines outline the eastern Pacific triangle and WP K-shaped regions where the mega-ENSO index is defined.

disappear. Instead, there is a deeper anomalous low over the Aleutian Islands and Gulf of Alaska. We also used the PDO and IPO indices regressed to the Z500 anomalies in both epochs and found that there is no significant difference. Thus, the PDO and IPO may not be key factors leading to interdecadal variations in the WP and AL patterns.

To explore the possible origin of the differences in the circulation, the SSTAs associated with ENSO in the two epochs are compared (Fig. 6). In both epochs, significant positive SSTAs are located over the equatorial eastern Pacific Ocean. But during P2 (Fig. 6b), the SSTAs in the Pacific are out of

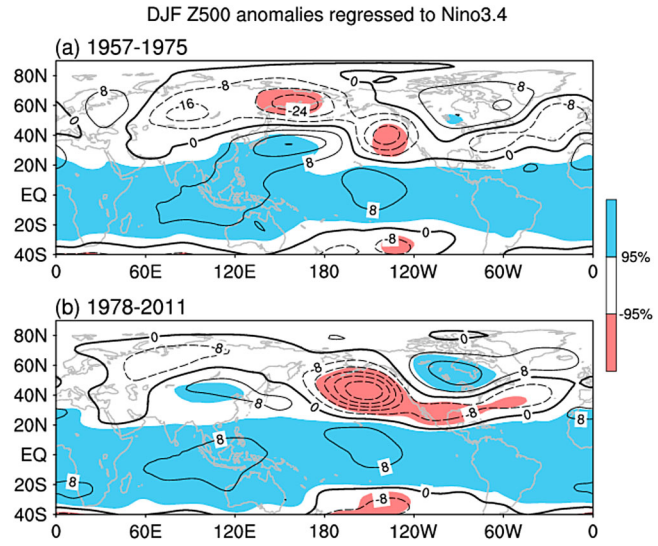

Fig. 5 The DJF Z500 (contour intervals are 8 gpm) pattern regressed against the Niño 3.4 index for (a) the 1957–1975 and (b) the 1978–2011 periods. Values in the shaded areas exceed the 95% confidence level.

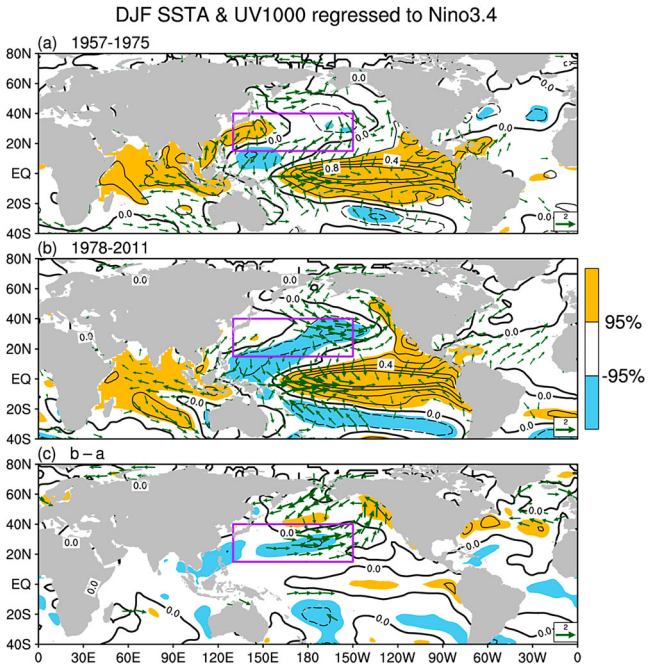

Fig. 6 DJF SSTA (contour intervals are 0.2 K) and 1000 hPa wind anomalies (vector units m s^{-1}) regressed against the normalized Niño 3.4 index for (a) 1957–1975; (b) 1978–2011; (c) shows (b) minus (a). Values in the shaded areas or wind vectors plotted in (a) and (b) exceed the 95% confidence level, while those in (c) indicate SSTAs above 0.12 K or below −0.12 K and wind vectors above 0.8 m s^{-1}. The SSTAs averaged inside the area outlined in the purple box (130°E–150°W, 15°–40°N) is defined as an XNP index (XNPI).

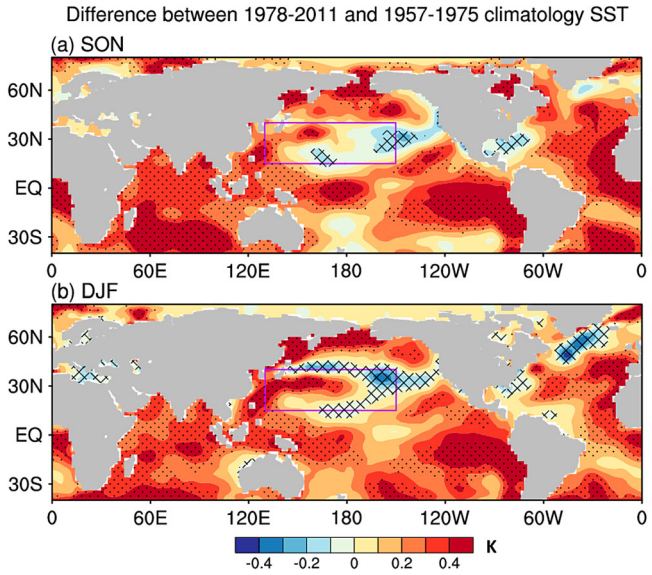

Fig. 7 (a) SON and (b) DJF climatology SST difference between 1978–2011 and 1957–1975. The dotted and crossed areas represent values exceeding the 95% confidence level. The area outlined in purple denotes the XNP area.

phase in the east–west direction, which resembles an ENSO pattern but with larger spatial ranges into the extratropical latitudes. As proposed by Wang et al. (2013), the SSTA pattern across the Pacific during P2 is similar to the spatial structure of a mega-ENSO. A major difference between the two epochs lies in the extratropical Pacific (Fig. 6c). In this study, we pay more attention to the XNP region (area outlined in purple in Fig. 6). During P2, significant negative SSTAs usually emerge in the XNP region during a warm ENSO winter (Fig. 6b), but the positive SSTAs in the western XNP are more significant during P1 (Fig. 6a) than those during P2. If the SSTAs averaged within the boxed area (130°E–150°W, 15°–40°N) in the XNP region is defined as an index (XNPI), the correlation with Niño 3.4 is −0.28 for P1 and −0.47 (above the 95% confidence level based on a Student's *t*-test) for P2. Such an interdecadal change in the North Pacific SSTAs can also be discerned during the preceding September, October, and November (SON) (figure not shown).

Figure 7 shows the difference in climatological SSTs between these two epochs for SON and DJF. The patterns with significant SST differences over the North Pacific (Figs 7a and 7b) are similar. The region with significant SSTAs in DJF, however, is larger than that in SON. However, the east–west dipole SSTA pattern in the outlined region is not in agreement with Fig. 6c. From Figs 6 and 7, we may speculate that the change in the XNP SSTAs from P1 to P2 may not be caused by the conversion of climatological SSTs but by the interdecadal change in ENSO. The ENSO-related SSTA structure in the Pacific Ocean shows a pattern resembling a mega-ENSO in P2 but a conventional ENSO pattern in P1. Next, we will discuss the modulating effect of XNP SSTAs.

5 The modulating effect of the XNP and numerical experiments

a *The modulating effect of the XNP*

The relationship between XNPI and Pacific SSTAs in P1 and P2 is depicted in Fig. 8. During P2 (Fig. 8b), significant negative SSTAs are observed over the western and

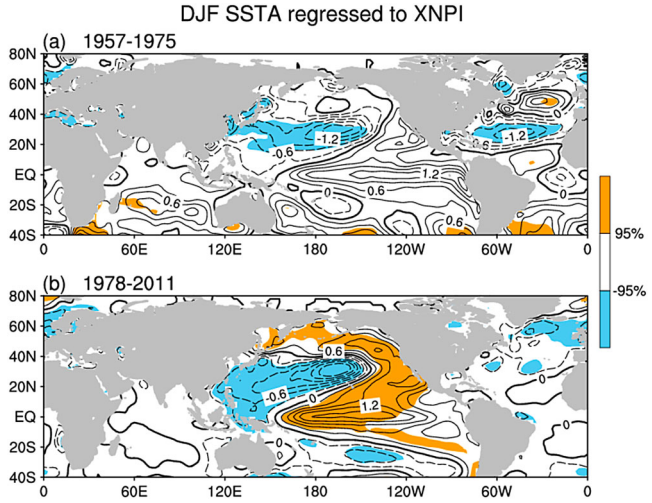

Fig. 8 The DJF SSTA (contours intervals are 0.3 K) pattern regressed against the XNPI for (a) the 1957–1975 and (b) the 1978–2011 periods. Values in the shaded areas exceed the 95% confidence level.

extratropical Pacific in both hemispheres, with certain significant positive SSTAs appearing over the eastern Pacific. This is in agreement with the defined regions of a mega-ENSO (shown in Fig. 4b). In contrast to P2, there is no significant SSTA pattern resembling ENSO appearing in P1, although the XNP SSTA pattern still exists (Fig. 8a). These conditions reflect the fact that the XNP had a synergistic effect with the tropical eastern Pacific from 1978 to 2011. Such a relationship is not obvious in the years before 1975. Thus, 1957–1975 can be considered as a conventional ENSO forcing period and 1979–2012 as a mega-ENSO forcing period. Next, the Z500 anomalies are regressed against XNPI (Fig. 9) to examine the effect of the XNP SSTAs, which show a pattern of Z500 anomalies similar to an AL and are also similar to the spatial pattern in the Fig. 5b (PCC = 0.9, in the region 20°–80° N, 180°–120°W). In order to examine whether XNP SSTAs could exert an effect without ENSO, a partial-regression approach was used to remove the ENSO signal from XNP (Fig. 10). Compared with Fig. 9, no significant Z500 anomaly exists over the tropical region. The significant negative anomalies stretch from the mid-latitude eastern Pacific as far westward as East Asia; the significant positive anomalies shift southwestward and become located over eastern Siberia. In general, corresponding to the negative XNP SSTAs, the Z500 anomaly over the western North Pacific exhibits a pattern similar to the positive phase of the WP pattern, which is opposite to that in Fig. 5a (PCC = −0.83, in the region 20°–80°N, 120°E–180°).

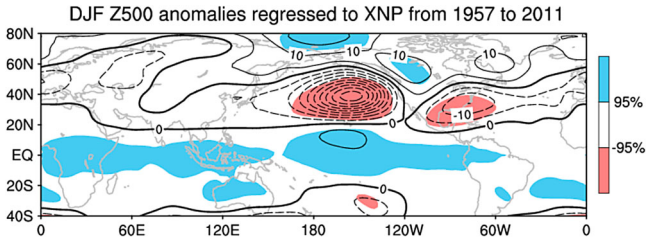

Fig. 9 DJF Z500 anomalies regressed against the XNPI (contour intervals are 5 gpm). Values in the shaded areas exceed the 95% confidence level.

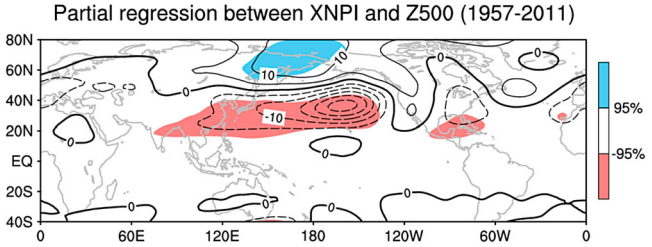

Fig. 10 Partial regression between Z500 and the XNPI with the Niño 3.4 index signal removed (contour intervals are 5 gpm). Values in the shaded areas exceed the 95% confidence level.

The results presented above indicate that, during the 1978–2011 period, the leading mode of North Pacific circulation variability, conventionally defined as the AL, may owe its existence to a superposition of two patterns. A negative–positive dipole Z500 anomaly mode, which is associated with the negative XNP SSTAs, located over mid- and high-latitude regions and throughout the entire North Pacific Ocean. The dipole mode projects upon the tropical forced negative phase of the WP signature, resulting in the generation of the AL. Thus, the AL during P2 may be a reflection of a tropical–extratropical (equatorial eastern Pacific–XNP) SSTA coupling effect. Specifically, during a warm conventional ENSO event, a negative phase of the WP pattern and a weak anomalous low would appear over the western and eastern North Pacific separately (Figs 5a and 6a). Accompanied by the significant negative SSTAs appearing in the XNP region, the SSTA pattern across the Pacific is similar to the spatial structure of a mega-ENSO (Fig. 6b). Because of the previously mentioned superposition, the negative–positive dipole Z500 anomaly mode would balance the negative phase of the WP pattern, resulting in WP-neutral Z500 anomalies over the western North Pacific. On the other hand, the significant negative anomalies are superimposed on the weak anomalous low over the eastern Pacifc, which results in an enhaced anomalous AL pattern.

b *Numerical experiments*

Diverse results have been produced by many studies, and no conclusive relationship has been recognized between extratropical SSTs and atmospheric circulation (e.g., Lau & Nath, 1990, 1996; Peng, Robinson, & Hoerling, 1997; Ting & Wang, 1997). Some studies have pointed out that the variability of extratropical North Pacific SSTs is a response to the overlying atmosphere, while others have indicated that the SSTs can force, or at least provide feedback to, the atmospheric circulation. As Robinson (2000) claimed, the atmospheric response to extratropical SSTAs is weak but not negligible.

The regression analysis does not infer any cause-and-effect relationship between the extratropical circulation and XNP SSTAs. To verify whether the underlying XNP SSTAs can force the atmospheric circulation or not and to elucidate the different impacts of conventional ENSO-like and mega-ENSO-like SSTAs on the teleconnections over the North Pacific, we performed the following numerical experiments with the ECHAM5.4 model. The details of the design of the experiments can be seen in Section 2.

The model responses of Z500 and the wind at 1000 hPa (UV1000) to mega-ENSO SSTA forcing are shown in Fig. 11a (mega-ENSO forcing minus control run). Affected by negative SSTAs in the XNP region and positive SSTAs in the equatorial eastern Pacific, the westerly flow is reinforced over the XNP region and a negative anomaly centre similar to the AL is located over the Gulf of Alaska and the Aleutian

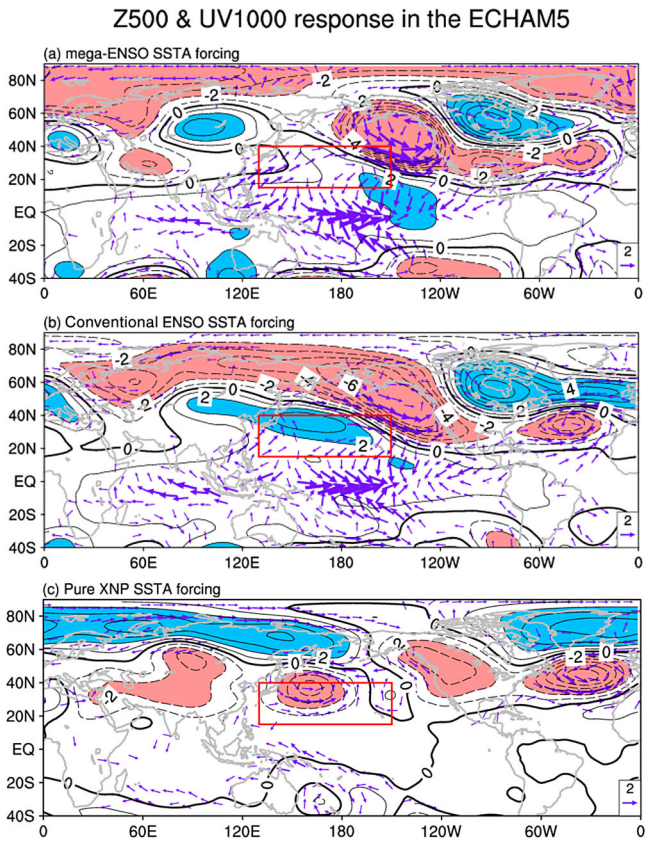

Fig. 11 (a) DJF Z500 (contour intervals are 1 gpm 10^{-1}) and UV1000 (vectors in m s^{-1}) responses in ECHAM5 regarding the difference between mega-ENSO forcing and the control run. (b) As in (a) but with XNP forcing removed. (c) As in (a) but using pure XNP forcing without ENSO forcing. The shaded areas indicate Z500 values above 2 gpm x 10^{-1} or below −2 gpm x 10^{-1} and wind vectors above 0.8 m s^{-1}.

Islands. This is similar to observations (Fig. 5b and wind field in Fig. 6b). However, when forced by a conventional ENSO (without XNP SSTAs), the westerly flow moved northward while the low pressure in the Aleutian region extended westward. A Z500 anomaly similar to the WP pattern appeared over the western North Pacific (Fig. 11b), which is similar to the spatial pattern shown in Fig. 5a and the wind field pattern in Fig. 6a. In agreement with observations (Fig. 10b), the Z500 anomaly pattern in Fig. 11c is similar to the positive phase of the WP pattern with high pressure anomalies located over the high-latitude western North Pacific region and low-pressure anomalies over mid-latitudes in response to the negative XNP SSTA forcing. Over the eastern North Pacific, there is a small difference between the observations and simulation. Comparing Fig. 11c with Fig. 10, an anomalous high appears instead of the anomalous low. The reason for this needs further study. But the present modelling results are in good agreement with the observational results derived before. When mega-ENSO type SSTAs are seen in the Pacific Ocean, the negative XNP SSTA would excite a negative–positive dipole Z500 anomaly mode. The dipole mode could balance out the negative phase of the WP, which is associated with the conventional ENSO, resulting in a WP-neutral Z500 anomaly pattern over the western North Pacific and an anomalous pattern over the eastern North Pacific similar to the AL.

6 Conclusions and discussion

This study compares the correlation between ENSO and North Pacific atmospheric circulation during boreal winters between 1958–1975 and 1978–2011. We found that the connection between ENSO and the WP and AL patterns has experienced a notable interdecadal change. During the 1957–1975 period, in the mature phase of ENSO, significant SSTAs occurred mainly in the equatorial eastern Pacific Ocean and the associated atmospheric circulation anomalies resembled the negative phase of the WP pattern. In contrast, for the 1978–2011 period, significant negative SSTAs were observed over the western and extratropical Pacific in both hemispheres, with certain significant positive SSTAs appearing over the eastern Pacific. This is in agreement with the defined regions of a mega-ENSO. The accompanying atmospheric circulation pattern shows a significant anomalous pattern similar to the AL rather than the WP pattern over the North Pacific.

Lau and Nath (1990) and Alexander, Lau, and Scott (2004) suggested that the extratropical northwestern Pacific SSTAs associated with ENSO events are forced by the atmosphere rather than vice versa. However, Zhang et al. (1996) found that the dominant patterns in the extratropical atmosphere and SSTs were still strongly coupled even without the influence of ENSO, which implies that the extratropical northwestern Pacific SSTAs can be independent of the ENSO-related atmospheric anomalies. Wu and Lin (2012) also found that a poleward-propagating Rossby wavetrain, possibly enhanced by SSTAs in the extratropical North Pacific associated with the developing phases of ENSO, is responsible for connecting the ENSO signal with the North Atlantic Oscillation (NAO). Both observational and modelling analyses in this study further confirm that the negative XNP SSTAs can excite a negative–positive dipole Z500 anomaly mode that would balance the negative phase of WP related to a conventional ENSO, resulting in WP-neutral Z500 anomalies over the western North Pacific and an anomalous AL-like pattern over the eastern North Pacific. But such interdacadel changes in the relationship between tropical and extratropical SSTAs and the North Pacific atmospheric circulation cannot be detected by using either the PDO or IPO indices. Thus, ENSO, rather than the PDO or IPO, is the key factor responsible for the interdecadal variation of the WP pattern and the AL.

It should be pointed out that the XNP SSTAs are not simply associated with ENSO. Although the correlation coefficient between ENSO and the XNP index reaches −0.45, ENSO can only explain 20% of the total XNP SST variance. For instance, XNP SSTAs are also related to extratropical North Atlantic SSTAs (area outlined in red in Fig. 12). Some studies have also found that Atlantic SSTAs influence the

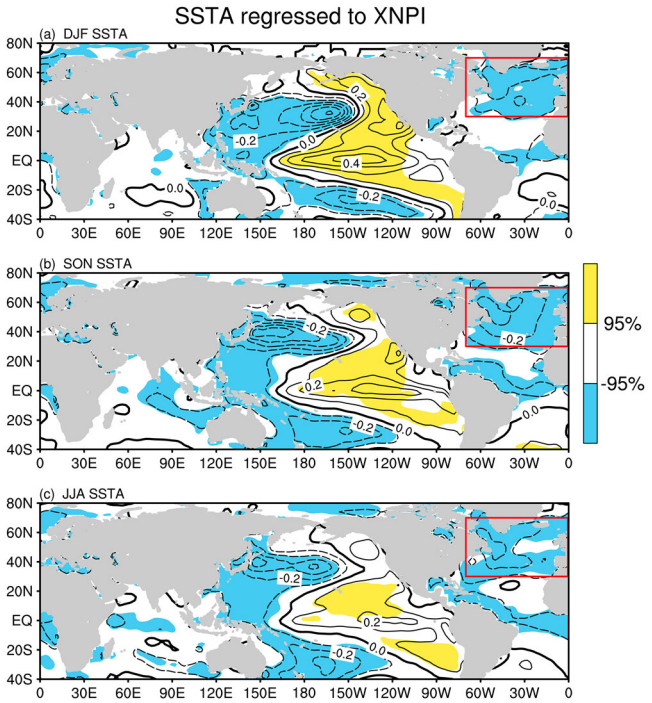

Fig. 12 (a) DJF, (b) SON, and (c) JJA SSTAs (contour intervals are 0.1 K) regressed against XNPI. Values in the shaded areas exceed the 95% confidence level. The area outlined in red indicates the extratropical North Atlantic SSTAs.

Pacific Ocean. Ham, Kug, Park, and Jin (2013) pointed out that tropical North Atlantic SSTs could be seen as a trigger for ENSO events. The off-equatorial North Atlantic SSTAs were linked to both North Atlantic variability (Okumura, Xie, Numaguti, & Tanimoto, 2001; Watanabe & Kimoto, 1999) and ENSO (Alexander & Scott, 2002; Klein, Soden, & Lau, 1999). Thus, whether Atlantic SSTAs affect the XNP directly or through ENSO is still unknown, and determining the origin of XNP SSTAs requires further theoretical and numerical studies.

Last but not least, many studies have pointed out that ENSO is still the most predictable climatic signal (Cheng, Tang, & Chen, 2011; Kirtman & Schopf, 1998) in relation to both the East Asian winter monsoon (EAWM) and the East Asian summer monsoon (EASM). These were shown to be modulated by the PDO (Chan & Zhou, 2005; Wang et al., 2008) and IPO (Lee, Kim, Jhun, Ha, & Seo, 2013). As an integrated measure of ENSO, PDO, and IPO, the mega-ENSO index was also used as a predictor for predicting EASM, yielding promising results (Wang et al, 2013; Wu & Yu, 2015). Recently, Jia, Lin, and Ge (2015) showed that the second empirical orthogonal function (EOF2) of surface air temperature (SAT) over East Asia is associated with notably different circulation patterns before and after the mid-1980s. In the North Pacific, a large-scale low-pressure anomaly was associated with the EOF2 of SAT before the mid-1980s. However, a negative PNA-like pattern appeared after the mid-1980s associated with the EOF2 of SAT. Our results show that an SSTA pattern similar to a mega-ENSO may exert its effect on EAWM by exciting a PNA-like pattern (AL) during P2 (Fig. 5b). Thus, an ENSO with different spatial patterns may change its link with the EAWM or North American winter climate through modulating the North Pacific atmospheric circulation. This highlights the importance of examining how ENSO influences North Pacific circulation patterns, such as WP or AL patterns.

Acknowledgements

We thank Drs. Guosen Chen and Zhiqing Xu for helpful discussions.

Disclosure statement

No potential conflict of interest was reported by the authors.

Funding

This work was jointly supported by the National Natural Science Foundation of China through Grant numbers [91437216, 91637312, and 41575075], the Ministry of Science and Technology of China through Grant numbers [2016YFA0601801, 2015CB453201, and 2015CB953904], the Public Science and Technology Research Funds projects of ocean through Grant number [201505013], and the Innovation Project of Jiangsu Province through Grant number [1344051501004].

References

Alexander, M. A., Lau, N.-C., & Scott, J. D. (2004). Broadening the atmospheric bridge paradigm: ENSO teleconnections to the tropical West Pacific–Indian Oceans over the seasonal cycle and to the North Pacific in summer. In C. Wang, S. P. Xie, & J. Carton (Eds.), *Earth's climate: The ocean–atmosphere interaction, AGU monograph* (Vol. 147, pp. 85–104), Washington, DC: American Geophysical Union. doi:10.1029/147GM05

Alexander, M. A., & Scott, J. D. (2002). The influence of ENSO on air-sea interaction in the Atlantic. *Geophysical Research Letters*, *29*(14). 46-1–46-4, doi:10.1029/2001GL014347

Anderson, B. T., Furtado, J. C., Kim, M. C., & Di Lorenzo, E. (2013). Extratropical forcing of El Niño-Southern Oscillation asymmetry. *Geophysical Research Letters*, *40*(18), 4916–4921.

Anderson, B. T., & Renellys, C. P. (2015). ENSO and non-ENSO induced charging and discharging of the equatorial Pacific. *Climate Dynamics*. *45*(9), 2309–2327, doi:10.1007/s00382-015-2472-x

Barlow, M., Nigam, S., & Berbery, E. H. (2001). ENSO, Pacific decadal variability, and U.S. summertime precipitation, drought, and stream flow. *Journal of Climate*, *14*, 2105–2128.

Bjerknes, J. (1966). A possible response of the atmospheric Hadley circulation to equatorial anomalies of ocean temperature. *Tellus*, *18*, 820–829.

Bjerknes, J. (1969). Atmospheric teleconnections from the equatorial Pacific. *Monthly Weather Review*, *97*, 163–172.

Bretherton, C. S., Widmann, M., Dymnikov, V. P., Wallace, J. M., & Blade, I. (1999). Effective number of degrees of freedom of a spatial field. *Journal of Climate*, *12*, 1990–2009.

Ceballos, L. I., Di Lorenzo, E., Hoyos, C. D., Schneider, N., & Taguchi, B. (2009). North Pacific gyre oscillation synchronizes climate fluctuations in the eastern and western boundary systems. *Journal of Climate*, *22*, 5163–5174.

Chan, J. C. L., & Zhou, W. (2005). PDO, ENSO and the early summer monsoon rainfall over south China. *Geophysical Research Letters*, *32*, L08810. doi:10.1029/2004GL022015

Chang, C.-P., Zhang, Y., & Li, T. (2000). Interannual and interdecadal variation of the East Asian summer monsoon rainfall and tropical SSTs. Part 1: Roles of the subtropical ridge. *Journal of Climate*, *13*, 4310–4325.

Charney, J. G., & Shukla, J. (1981). Predictability of monsoons. In J. Lighthill & R. P. Pearce (Eds.), *Monsoon dynamics* (pp. 99–109). New York: Cambridge University Press.

Cheng, Y., Tang, Y., & Chen, D. (2011). Relationship between predictability and forecast skill of ENSO on various time scales. *Journal of Geophysical Research*, *116*, C12006. doi:10.1029/2011JC007249

Compo, G. P., Whitaker, J. S., & Sardeshmukh, P. D. (2006). Feasibility of a 100-year reanalysis using only surface pressure data. *Bulletin of the American Meteorological Society*, *87*, 175–190.

Compo, G. P., Whitaker, J. S., Sardeshmukh, P. D., Matsui, N., Allan, R. J., Yin, X., … Worley, S. J. (2011). The twentieth century reanalysis project. *Quarterly Journal of the Royal Meteorological Society*, *137*, 1–28.

Dai, A. G. (2013). The influence of the interdecadal Pacific oscillation on US precipitation during 1923–2010. *Climate Dynamics*, *41*, 633–646.

Deser, C., Alexander, M. A., & Timlin, M. (1996). Upper-ocean thermal variations in the North Pacific during 1970–1991. *Journal of Climate*, *9*, 1840–1855.

Deser, C., Alexander, M. A., & Timlin, M. (1999). Evidence for a wind-driven intensification of the Kuroshio current extension from the 1970s to the 1980s. *Journal of Climate*, *12*, 1697–1706.

Ding, R., Ha, K., & Li, J. (2010). Interdecadal shift in the relationship between the East Asian summer monsoon and the tropical Indian Ocean. *Climate Dynamics*, *34*, 1059–1071. doi:10.1007/s00382-009-0555-2

Gong, D. Y., Wang, S. W., & Zhu, J. H. (2001). East Asian winter monsoon and Arctic Oscillation. *Geophysical Research Letters*, *28*(10), 2073–2076.

Graham, N. E. (1994). Decadal-scale climate variability in the tropical and North Pacific during the 1970s and 1980s: Observations and model results. *Climate Dynamics*, *10*, 135–162.

Guilderson, T. P., & Schrag, D. P. (1998). Abrupt shift in subsurface temperatures in the tropical Pacific associated with changes in El Niño. *Science*, *281*, 240–243. doi:10.1126/science.281.5374.240

Ham, Y. G., Kug, J. S., Park, J. Y., & Jin, F. F. (2013). Sea surface temperature in the north tropical Atlantic as a trigger for El Niño/Southern Oscillation events. *Nature Geoscience*, *6*, 112–116.

Hanawa, K., Ishizaki, S., & Tanimoto, Y. (1996). Strengthening of wintertime mid-latitude westerlies over the North Pacific since mid-1970s. *Journal of the Meteorological Society of Japan*, *74*, 715–721.

He, S. P., & Wang, H. J. (2013). Oscillating relationship between the East Asian winter monsoon and ENSO. *Journal of Climate*, *26*, 9819–9838.

He, S. P., Wang, H. J., & Liu, J. P. (2013). Changes in the relationship between ENSO and Asia Pacific midlatitude winter atmospheric circulation. *Journal of Climate*, *26*, 3377–3393.

Hoell, A., & Funk, C. (2013). The ENSO-related west Pacific sea surface temperature gradient. *Journal of Climate*, *26*(23), 9545–9562.

Horel, J. D., & Wallace, J. M. (1981). Planetary-scale atmospheric phenomena associated with the Southern Oscillation. *Monthly Weather Review*, *109*, 813–829.

Hsu, H. H., & Wallace, J. D. (1985). Vertical structure of winter-time teleconnection patterns. *Journal of the Atmospheric Sciences*, *42*, 1693–1710.

Jia, X., Lin, H., & Ge, J. (2015). The interdecadal change of ENSO impact on wintertime East Asian climate. *Journal of Geophysical Research Atmospheres*, *120*(11), 918–11,935. doi:10.1002/2015JD023583

Jin, F. F., Neelin, J. D., & Ghil, M. (1994). El Niño on the devil's staircase: Annual subharmonic steps to chaos. *Science*, *264*, 70–72.

Kim, B.-H., & Ha, K.-J. (2015). Observed changes of global and western Pacific precipitation associated with global warming SST mode and mega-ENSO SST mode. *Climate Dynamics*, *45*, 3067–3075. doi:10.1007/s00382-015-2524-2

King, A. D., Alexander, L. V., & Donat, M. G. (2013). Asymmetry in the response of Eastern Australia extreme rainfall to low frequency Pacific variability. *Geophysical Research Letters*, *40*, 2271–2277. doi:10.1002/grl.50427

Kirtman, B. P., & Schopf, P. S. (1998). Decadal variability in ENSO predictability and prediction. *Journal of Climate*, *11*, 2804–2822.

Klein, S. A., Soden, B. J., & Lau, N. C. (1999). Remote sea surface temperature variations during ENSO: Evidence for a tropical atmospheric bridge. *Journal of Climate*, *12*, 917–932.

Kodera, K. (1998). Consideration of the origin of the different midlatitude atmospheric responses among El Niño events. *Journal of the Meteorological Society of Japan*, *76*, 347–361.

Kodera, K., Chiba, M., Koide, H., Kitoh, A., & Nikaidou, Y. (1996). Interannual variability of the winter stratosphere and troposphere in the Northern Hemisphere. *Journal of the Meteorological Society of Japan*, *74*(3), 365–382.

Latif, M., & Barnett, T. P. (1994). Causes of decadal climate variability over the North Pacific and North America. *Science*, *266*, 634–637.

Latif, M., & Barnett, T. P. (1996). Decadal climate variability over the North Pacific and North America: Dynamics and predictability. *Journal of Climate*, *9*, 2407–2423.

Lau, N.-C., & Nath, M. J. (1990). A general circulation model study of the atmospheric response to extratropical SST anomalies observed in 1950–79. *Journal of Climate*, *3*, 965–989.

Lau, N.-C., & Nath, M. J. (1996). The role of the "atmospheric bridge" in linking tropical Pacific ENSO events to extratropical SST anomalies. *Journal of Climate*, *9*, 2036–2057.

Lee, S.-S., Kim, S.-H., Jhun, J.-G., Ha, K.-J., & Seo, Y.-W. (2013). Robust warming over East Asia during boreal winter monsoon and its possible causes. *Environmental Research Letters*, *8*(3), 034001. doi:10.1088/1748-9326/8/3/034001

Linkin, M. E., & Nigam, S. (2008). The North Pacific Oscillation–West Pacific teleconnection pattern: Mature-phase structure and winter impacts. *Journal of Climate*, *21*, 1979–1997.

Mantua, N. J., Hare, S. R., Zhang, Y., Wallace, J. M., & Francis, R. C. A., 1997. Pacific interdecadal climate oscillation with impacts on salmon production. *Bulletin of the American Meteorological Society*, *78*, 1069–1079.

Maslanik, J. A., Serreze, M. C., & Barry R. G. (1996). Recent decreases in Arctic summer ice cover and linkages to atmospheric circulation anomalies. *Geophysical Research Letters*, *23*, 1677–1680.

Mo, K. C., & Livezey, R. E. (1986). Tropical-extratropical geopotential height teleconnections during the northern hemisphere winter. *Monthly Weather Review*, *114*, 2488–2515.

Neelin, J. D., Battisti, D. S., Hirst, A. C., Jin, F. F., Wakata, Y., Yamagata, T., & Zebiak, S. (1998). ENSO theory. *Journal of Geophysical Research: Oceans*, *103*(C7), 14261–14290.

Nigam. (2003). Teleconnections. In J. R. Holton J. Pyle, & J. A. Curry (Eds.), *Encyclopedia of atmospheric sciences* (pp. 2243–2269). Salt Lake City: Academic Press.

Okumura, Y., Xie, S.-P., Numaguti, A., & Tanimoto, Y. (2001). Tropical Atlantic air-sea interaction and its influence on the NAO. *Geophysical Research Letters*, *28*, 1507–1510.

Oshika, M., Tachibana, Y., & Nakamura, T. (2014). Impact of the winter North Atlantic Oscillation (NAO) on the Western Pacific (WP) pattern in the following winter through Arctic sea ice and ENSO: Part I—observational evidence. *Climate Dynamics*, *45*, 1355–1366. doi:10.1007/s00382-014-2384-1

Overland, J. E., Adams, J. M., & Bond, N. A. (1999). Decadal variability of the Aleutian Low and its relation to high-latitude circulation. *Journal of Climate*, *12*, 1542–1548.

Peng, S. L., Robinson, W. A., & Hoerling, M. P. (1997). The modeled atmospheric response to midlatitude SST anomalies and its dependence on background circulation states. *Journal of Climate*, *10*, 971–987.

Robinson, W. A. (2000). Review of WETS–The Workshop on Extra-Tropical SST anomalies. *Bulletin of the American Meteorological Society*, *81*, 567–577. doi:10.1175/1520-0477(2000)081<0567:ROWTWO>2.3.CO;2

Roeckner, E., Bäuml, G., Bonaventura, L., Brokopf, R., Esch, M., Giorgetta, M., … Tompkins, A. (2003). The atmospheric general circulation model ECHAM5: Part I: Model description. Max Planck Institute, Rep. Report No. 349.

Rogers, J. C. (1981). The North Pacific Oscillation. *Journal of Climatology*, *1*, 39–57.

Ropelewski, C. F., & Halpert, M. S. (1986). North American precipitation and temperature patterns associated with the El Niño/Southern Oscillation (ENSO). *Monthly Weather Review*, *114*, 2352–2362.

Smith, T. M., Reynolds, R. W., Peterson, T. C., & Lawrimore, J. (2008). Improvements to NOAA's historical merged land–ocean surface temperature analysis (1880–2006). *Journal of Climate*, *21*, 2283–2296.

Ting, M. F., & Wang, H. (1997). Summertime U.S. precipitation variability and its relation to Pacific sea surface temperature. *Journal of Climate*, *10*, 1853–1873.

Trenberth, K. E. (1990). Recent observed interdecadal climate changes in the northern hemisphere. *Bulletin of the American Meteorological Society*, *71*, 988–993.

Trenberth, K. E., & Hurrell, J. W. (1994). Decadal atmosphere-ocean variations in the Pacific. *Climate Dynamics*, *9*, 303–319.

Trenberth, K. E., & Smith, L. (2009). Variations in the three-dimensional structure of the atmospheric circulation with different flavors of El Niño. *Journal of Climate*, *22*(11), 2978–2991.

Walker, G., & Bliss, E. (1932). World weather. *V, Memoirs of the Royal Meteorological Society*, *4*, 53–84.

Wallace, J. M., & Gutzler, D. (1981). Teleconnections in the geopotential height field during the northern hemisphere winter. *Monthly Weather Review*, *109*, 784–812.

Wang, B., Liu, J., Kim, H. J., Webster, P. J., Yim, S. Y., & Xiang, B. Q. (2013). Northern hemisphere summer monsoon intensified by mega-El Niño/Southern Oscillation and Atlantic multidecadal oscillation. *Proceedings of the National Academy of Sciences*, *110*, 5347–5352.

Wang, B., Wu, R. G., & Fu, X. H. (2000). Pacific–East Asia teleconnection: How does ENSO affect East Asian climate? *Journal of Climate*, *13*, 1517–1536.

Wang, B., Wu, Z. W., Li, J. P., Liu, J., Chang, C.-P., Ding, Y. H., & Wu, G. X. (2008). How to measure the strength of the East Asian summer monsoon? *Journal of Climate*, *21*, 4449–4463.

Wang, H., & Kumar, A. (2015). Assessing the impact of ENSO on drought in the U.S. Southwest with NCEP climate model simulations. *Journal of Hydrology*, *526*, 30–41.

Wang, L., Chen, W., & Huang, R. (2008). Interdecadal modulation of PDO on the impact of ENSO on the East Asian winter monsoon. *Geophysical Research Letters*, *35*, L20702. doi:10.1029/2008GL035287

Wang, X., Feng, Y., Compo, G. P., Swail, V. R., Zwiers, F. W., Allan, R. J., & Sardeshmukh, P. D. (2013). Trends and low frequency variability of extra-tropical cyclone activity in the ensemble of twentieth century reanalysis. *Climate Dynamics*, *40*, 2775–2800. doi:10.1007/s00382-012-1450-9

Watanabe, M., & Kimoto, M. (1999). Tropical-extratropical connection in the Atlantic atomosphere-ocean variability. *Geophysical Research Letters*, *26*, 2247–2250.

Whitaker, J. S., Compo, G. P., Wei, X., & Hamill, T. M. (2004). Reanalysis without radiosondes using ensemble data assimilation. *Monthly Weather Review*, *132*, 1190–1200.

Wu, Z., & Li, J. (2008). Prediction of the Asian-Australian monsoon interannual variations with the grid-point atmospheric model of IAP LASG (GAMIL). *Advances in Atmospheric Sciences*, *25*(3), 387–394.

Wu, Z., & Li, J. (2009). Seasonal prediction of the global precipitation annual modes with the grid-point atmospheric model of IAP LASG (GAMIL). *Acta Meteorologica Sinica*, *23*(4), 428–437.

Wu, Z., & Lin, H. (2012). Interdecadal variability of the ENSO-North Atlantic Oscillation connection in boreal summer. *Quarterly Journal of the Royal Meteorological Society*, *138*, 1668–1675.

Wu, Z., Wang, B., Li, J., & Jin, F. F. (2009). An emperical seasonal prediction model of the East Asian summer monsoon using ENSO and NAO. *Journal of Geophysical Research*, *114*, D18120. doi:10.1029/2009JD011733

Wu, Z., & Yu, L. (2015). Seasonal prediction of the East Asian summer monsoon with a partial-least square model. *Climate Dynamics*, *46*, 3067–3078. doi:10.1007/s00382-015-2753-4

Wu, Z., & Zhang, P. (2014). Interdecadal variability of the mega-ENSO–NAO synchronization in winter. *Climate Dynamics*, *45*, 1117–1128. doi:10.1007/s00382-014-2361-8

Zhang, R. H., Sumi, A., & Kimoto, M. (1996). Impact of El Niño on the East Asia Monsoon: A diagnostic study of the '86/87 and '91/92 events. *Journal of the Meteorological Society of Japan*, *74*, 49–62.

Zhang, Y., Wallace, J. M., & Iwasaka, N. (1996). Is climate variability over the North Pacific a linear response to ENSO? *Journal of Climate*, *9*, 1468–1478.

Zhang, Z., Gong, D., Hu, M., Guo, D., He, X., & Lei, Y. (2009). Anomalous winter temperature and precipitation events in southern China. *Journal of Geographical Sciences 19*(4), 471–488.